

Huei-Ping Huang · Richard Seager · Yochanan Kushnir

The 1976/77 transition in precipitation over the Americas and the influence of tropical sea surface temperature

Received: 23 September 2004 / Accepted: 9 February 2005 / Published online: 11 May 2005
© Springer-Verlag 2005

Abstract Most major features of the interdecadal shift in boreal winter-spring precipitation over the American continents associated with the 1976–1977 transition are reproduced in atmospheric general circulation model (GCM) simulations forced with observed sea surface temperature (SST). The GCM runs forced with global and tropical Pacific SSTs produce similar multidecadal changes in precipitation, indicating the dominant influence of tropical Pacific SST. Companion experiments indicate that the shift in mean conditions in the tropical Pacific is responsible for these changes. The observed and simulated “post- minus pre-1976” difference in Jan–May precipitation is wet over Mexico and the southwest U.S., dry over the Amazon, wet over sub-African South America, and dry over the southern tip of South America. This pattern is not dramatically different from a typical El Niño-induced response in precipitation. Although the interdecadal (post- minus pre-1976) and interannual (El Niño–La Niña) SST anomalies differ in detail, they produce a common tropics-wide tropospheric warmth that may explain the similarity in the precipitation anomaly patterns for these two time scales. An analysis of local moisture budget shows that, except for Mexico and the southwest U.S. where the interdecadal shift in precipitation is balanced by evaporation, elsewhere over the Americas it is balanced by a shift in low-level moisture convergence. Moreover, the moisture convergence is due mainly to the change in low-level wind divergence that is linked to low-level ascent and descent.

1 Introduction

The influences of tropical sea surface temperature (SST) anomalies on the precipitation over the American continents on the interannual time scale are well known (Ropelewski and Halpert 1987). During El Niño, the southern edge of the U.S. and northern Mexico are typically wetter, northern Brazil and the Caribbean are drier, and southeastern South America is wetter than normal. The simultaneous occurrences of interannual climate anomalies in both hemispheres reflect their common origin in the tropical SST anomaly (Seager et al. 2003). Atmospheric general circulation models (GCMs) forced by El Niño SST anomalies have successfully simulated the inter-American precipitation pattern, an important basis for the two-tier system of seasonal prediction (e.g., Goddard et al. 2001). Looking for further evidence of the tropical control of midlatitude precipitation, recent studies have qualitatively reproduced prolonged North American droughts with atmospheric GCMs forced by observed tropical SST (Hoerling and Kumar 2003; Schubert et al. 2004; Seager et al. 2005, manuscript submitted to *J. Climate*). Following these developments, a natural and important extension that we will pursue in this study is to investigate the relationship between the interdecadal changes in tropical SST and precipitation over the Americas.

Unlike interannual variability that can be explained by recurring El Niños, the causes of multidecadal variability or trends in tropical SST remain a matter of investigation, with possibilities ranging from internal ocean–atmosphere dynamics (e.g., Gu and Philander 1997; McPhaden and Zhang 2002; Seager et al. 2004; Karspeck et al. 2004), changes in the characteristics of El Niño (Fedorov and Philander 2001), to greenhouse-gas forcing (e.g., Cane et al. 1997; Boer et al. 2004). Leaving the ocean dynamics aside, this work aims to investigate how the atmosphere and the precipitation over land in the American sector respond to the inter-

H.-P. Huang (✉) · R. Seager · Y. Kushnir
Lamont-Doherty Earth Observatory
of Columbia University, 61 Route 9W,
Palisades, NY, 10964 USA
E-mail: huei@ldeo.columbia.edu
Fax: +1-845-3658736

decadal changes in SST when the latter are given. The observed interdecadal changes in tropical SST and many atmospheric variables (e.g., global angular momentum, Huang et al. 2003; tropically averaged 200 hPa height, Kumar et al. 2004) for the second half of the twentieth century are not smooth but are distinguished by a “shift” in the late 1970s (Trenberth 1990), often called the 1976–1977 transition. The fact that the post- and pre-1976 periods have distinctive means provides a convenient setting for our investigation of the multi-decadal SST-precipitation relationship. Our strategy is to bypass an analysis of the detailed temporal evolution, containing all time scales, of the SST and precipitation for the second half of the twentieth century, and instead focus on the difference between the post- and pre-1976 epoch means. As an extension of previous GCM studies, we will determine whether an AGCM forced by the difference in tropical SST across the 1976 transition can simulate the corresponding interdecadal shift in precipitation over the Americas.

Using two GCMs different from the one used in the present study, Kumar et al. (2004) have recently looked at some aspects of the SST-precipitation relationship on the interdecadal time scale. They pointed out that, despite an increase in the tropics-wide temperature associated with the increase in tropical SST for 1950–2000, the precipitation over land in the tropics has decreased. This feature, which we will confirm, suggests that the change in precipitation could be more than just an intensification of the local recycling of water, namely, an increase in temperature leads to more evaporation that is balanced by more precipitation back to surface. As a new contribution to this problem, we will analyze not only the SST and precipitation, but also all terms in the local moisture budget associated with the 1976 transition. This will clarify whether the changes in regional precipitation are balanced by evaporation or by changes in atmospheric moisture transport. Due to deficiencies in the observations for atmospheric moisture field in the pre-1976 era (and a still large uncertainty in the decadal means of moisture in the post-satellite era, e.g., Allan et al. 2002), we will rely on GCM simulations for the moisture budget analysis.

Since some of the strongest El Niño events in the twentieth century occurred in the post-1976 period, the difference between the means of the post- and pre-1976 epochs could be due partly to the rectified effect of El Niño. Outside the tropical Pacific, the SSTs in other ocean basins may also influence the precipitation over the Americas. To shed light on these possibilities, we will analyze GCM simulations forced with global and tropical Pacific SSTs, and with the SST forcing including and excluding interannual variability (as detailed in Sect. 3). The basic features of the multidecadal changes in tropical SST are shown in Sect. 2. The model and GCM experiments are described in Sect. 3. The “post- minus pre-1976” differences in precipitation and moisture budget over the Americas are analyzed in Sect. 4, followed by additional discussions on the interdecadal

SST-precipitation relationship in Sects. 5, 6, and 7 and conclusions in Sec. 8.

2 SST and the 1976 transition

In this study, July 1961–June 1976 and July 1976–June 1998 are chosen to define the pre-1976 and post-1976 epochs. The choice of 1998 as the end of the post-76 era is guided by an apparent “reversal” of the post-1976 trend in the precipitation of the Americas that occurred in mid-1998 (see Sect. 7). The choice of 1961 as the other end point is somewhat arbitrary, but extending it to 1956 leads to qualitatively similar results in our GCM experiments (the “SCYC” runs to be discussed shortly). That these choices are meaningful is illustrated in Fig. 1a–c, the Jan–May SST “anomalies” (defined as the departure from the 1871–1999 climatology using the HadISST1 data set, Rayner et al. 2003) for the post- and pre-1976 periods and their difference. Both Fig. 1a and b exhibits a common pattern with the largest SST anomalies in the central/eastern Pacific and just south of the equator. Moreover, the post- and pre-1976 SST anomalies in Fig. 1a and b have the same pattern but opposite signs over most of the Indo-Pacific sector, rendering it meaningful to consider the two epochs the “positive” and “negative” phases of a multidecadal oscillation, with 1976 being the turning point.

The “post- minus pre-1976” SST difference field, shown in Fig. 1c, is positive over most of the Indo-Pacific sector, except for the two off-equatorial minima in the western Pacific. The most distinctive feature is, again, a maximum south of the equator in the central/

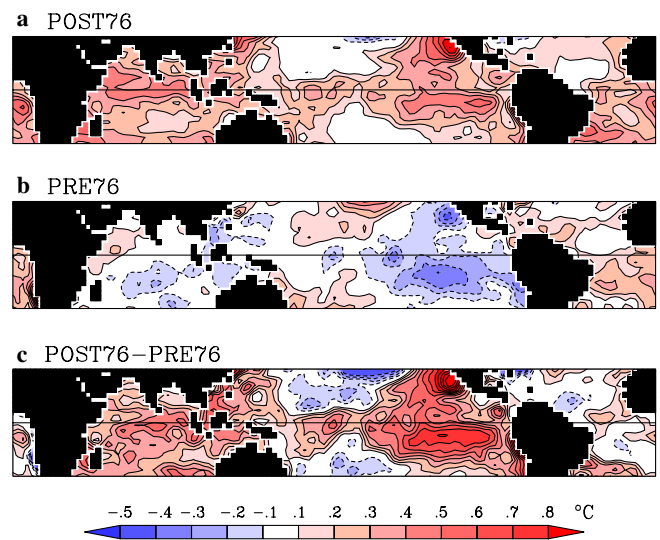


Fig. 1 The anomaly of Jan–May SST, defined as the departure from 1871–1999 long-term mean, for **a** post-1976 epoch (July 1976–June 1998), **b** pre-1976 epoch (July 1961–June 1976), **c** the difference of **a** and **b**. Contour interval 0.1°C, negative dashed. Areas with the absolute value of SST anomaly greater than 0.1°C are filled with *red* (positive) and *blue* (negative) colors

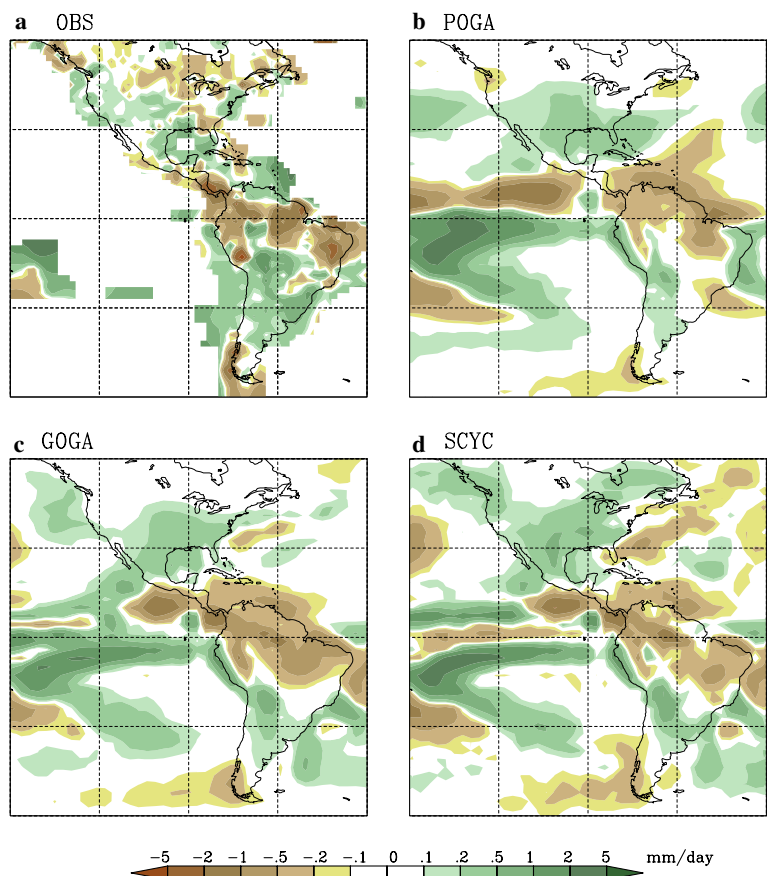
eastern Pacific. On the interannual time scale, El Niño in the equatorial Pacific influences the SST elsewhere through an “atmospheric bridge” (Alexander et al. 2001), producing SST anomalies of the same sign as the NINO3/3.4 index in the Indian Ocean and opposite sign in the North Pacific. Qualitatively, this remains true in Fig. 1c, but the Indian Ocean SST anomaly has become stronger relative to the NINO3/3.4 SST anomaly in the equatorial Pacific. These differences between the inter-annual and interdecadal SST anomaly patterns are also noted by Deser et al. (2004), who further showed the connection between the tropical and North Pacific oceans on the interdecadal time scale. The warming component in Fig. 1c also broadly resembles the SST trend simulated by some coupled GCMs forced with an increased greenhouse gas concentration (e.g., Knutson and Manabe 1995; Huang et al. 2001; Boer et al. 2004). The observed epoch difference in Fig. 1c could be a mixture of both internal variability and global warming trend.

To simplify the problem, the GCM simulations in this study will be forced by either tropical Pacific or global SSTs, without a further division into different basins. The interdecadal shift in SST has an annual cycle. To further narrow the focus, we will analyze the precipitation and moisture budget for the boreal winter–spring season.

3 Models and data

The AGCM used in this study is the National Center for Atmospheric Research (NCAR) Community Climate Model Version 3.10 (CCM3.10), with minimal modifications for executions on our local computing facilities. The model has 18 vertical levels and a T42 resolution. Three sets of GCM simulations are performed. The Pacific Ocean Global Atmosphere coupled with Mixed Layer ocean (POGA-ML) runs consist of 16 ensemble members for 1856–2000, with the model forced by observed SST over the tropical Pacific (including the western Pacific but excluding the Indian Ocean) and coupled to a simple mixed layer ocean elsewhere as detailed in Appendix 1. The global ocean global atmosphere (GOGA) runs include 48 ensemble members for 1959–1999 (16 members extended to 2004) forced by observed global SST. The 1961–1999 segments from the POGA-ML and GOGA runs are used in most of our analysis. The SCYC (abbreviation for “repeated seasonal cycle”) experiments consist of a pair of 30-year AGCM runs, each forced with a repeated seasonal cycle of global SST constructed from the means of the post- and pre-1976 epochs. The POGA-ML and GOGA runs produce substantial interannual variability due to El Niño. Compared to that, the interannual variability in the

Fig. 2 The “post- minus pre-1976” difference in Jan–May precipitation for **a** observation based on CAMS data set. **b** The 16-member ensemble average from the POGA-ML experiments. **c** The 48-member ensemble average from the GOGA runs. **d** Thirty-year average of the difference between a pair of the SCYC runs. Units are in mm/day with color scales indicated at the bottom. White areas are with insufficient data or with very weak signals (within ± 0.1 mm/day). All panels in Figs. 2, 3, 4, 5, 6 and 7, except Fig. 2a, are gently smoothed with a T31 filter (truncation at total wavenumber 31). The Domain shown is 150°W–30°W and 60°S–60°N



SCYC experiments consists of only internal variability that is further suppressed after a 30-year average.

Since long-term (including the pre-1976 era) observations of precipitation exist mainly over land, the verification of model simulations will be based on precipitation over the American continents. Unless otherwise noted, the CAMS station data interpolated onto a $2^\circ \times 2^\circ$ grid produced by NOAA Climate Prediction Center (<http://www.cpc.ncep.noaa.gov>) is used for precipitation.

4 Interdecadal shift in precipitation and moisture budget

Precipitation

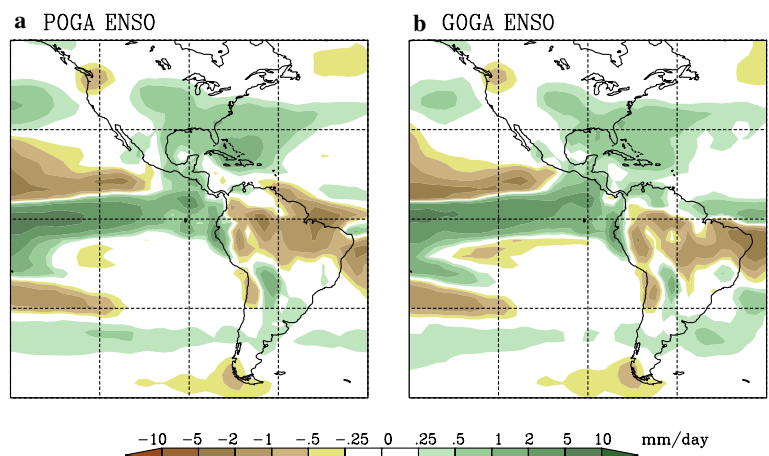
The “post- minus pre-1976” difference in Jan–May precipitation is shown in Fig. 2a–d for the observations and the POGA-ML, GOGA, and SCYC runs. The results for POGA-ML and GOGA are the ensemble average of 16 and 48 runs, respectively, while that for SCYC is the difference between a pair of 30-year perpetual post-1976 and pre-1976 runs. To first order, the GCM reproduces many observed features of the interdecadal shift in precipitation over the American continents, including dry anomalies over the Amazon and the southern tip of South America, wet anomalies over sub-Amazonian South America, Mexico, and the southwest U.S. Over these regions, the POGA-ML and GOGA runs produce very similar structures in precipitation, indicating the dominant impact of tropical Pacific SST. This result supports the emerging thought of the control of global climate by tropical oceans advanced by recent studies (Hoerling and Kumar 2003, Schneider et al. 2003; Seager et al. 2003; Schubert et al. 2004; Seager et al. 2005), although the emphases of these studies are not restricted to the Pacific (e.g., Hoerling and Kumar 2003 noted the contribution of the Indian Ocean SSTA to the post-1998 North American drought; Schneider et al. 2003 found a substantial influence of tropical Atlantic SST on the trend in precipitation over tropical

South America for the second half of the twentieth century). The SCYC runs, designed to exclude the rectified effect of interannual variability, also produce similar results in precipitation.

Despite the similarity between the POGA-ML and GOGA/SCYC runs, some second order differences are noticeable. For example, over the northeast coast of Brazil the precipitation anomalies are wet in POGA-ML but dry in GOGA, SCYC, and observations. These details might be related to the differences in the SSTs in the adjacent Atlantic Ocean (e.g., Giannini et al. 2004), i.e., the POGA-ML model simulation of tropical Atlantic SST anomalies is different from observations. Note as well a discrepancy between the simulated (for all three types of runs) and observed precipitation over the Great Lakes region and the northeast U.S., where the model is too wet during the post-1976 period. Otherwise, the rest of the simulated precipitation patterns in Fig. 2b–d are very robust, as they can be reproduced by retaining only a small number of ensemble members in the ensemble means for POGA-ML and GOGA, or a small number of years in the time mean for SCYC runs (not shown). A more detailed discussion on statistical significance is in Appendix 2.

Recalling that the canonical El Niño signal in precipitation is wet over the southern edge of the U.S., dry over northern South America, and wet over the central South America (Ropelewski and Halpert 1987), we note that in these regions the sign of the interannual signal is the same as the interdecadal one shown in Fig. 2. For a quick reference, the “warm minus cold” ENSO composite of Jan–May precipitation anomalies from the POGA-ML and GOGA runs is shown in Fig. 3. The similarity between the interdecadal and interannual precipitation signals is likely due to the broad similarity between the interdecadal and interannual (El Niño) SST anomalies, to be discussed further in Sect. 6. Nevertheless, there are non-trivial differences between the interannual and interdecadal precipitation patterns. In the latter, the wet anomaly in the southern edge of North America penetrates much deeper into the southwest

Fig. 3 The warm minus cold ENSO composite of Jan–May precipitation for the ensemble means of **a** POGA-ML runs. **b** GOGA runs. Color scales are indicated at the bottom. The composite is based on six major El Niños (Jan–May of 1966, 1969, 1983, 1987, 1992, and 1998) and six major La Ninas (1968, 1971, 1974, 1976, 1985, and 1989), normalized by the Jan–May average of NINO3.4 index. The composite is done after the time series of precipitation at each grid point is detrended with a high pass filter



U.S., while in the former it is centered to the southeast around the Gulf coast and Florida (Ropelewski and Halpert 1987). The dry region in the north, and wet region in central South America, are broader for the interdecadal anomalies. Also noteworthy is a dry anomaly over the southern tip of South America in both observed and simulated multidecadal precipitation patterns in Fig. 2. At first, it appears to be a unique feature of the interdecadal variability since it has not been recorded as part of the canonical ENSO signal in precipitation (Ropelewski and Halpert 1987). However, we did find a trace of dryness in this region in the simulated El Niño precipitation anomalies in the POGA-ML and GOGA runs. We postpone further comparisons of the interannual and interdecadal signals to Sects. 5 and 6.

Investigating the decadal variability (with period $T > 7$ years) of precipitation over land, Cayan et al. (1998; see their Fig. 10) found an apparent global correlation pattern for precipitation anomalies that broadly resembles our pattern of the multidecadal shift in the American sector. When the precipitation anomaly is wet in the southern/southwest U.S. and Mexico, it is dry/wet/dry over northern/central/southern South America. Using 6-year low-pass filtered data, Schubert et al. (2004, see their Fig. 2) also found a similar correlation pattern but with a diminished dry spot over the southern tip of South America. Although the frequency band consid-

ered by Cayan et al. (1998) and Schubert et al. (2004) for the low-frequency variability is broader (including fluctuations with relatively shorter periods) than ours, the partial overlap between the two may explain the similarity in the precipitation patterns. Most importantly, since we are able to simulate this inter-American precipitation pattern with the POGA-ML runs, the correlation between the precipitation anomalies in North and South America is likely due to the fact that they have a common origin in the tropical Pacific SST.

Moisture budget

In an equilibrium state, the local precipitation, P , can be related to the local moisture budget by

$$P = E - \{\nabla \cdot (\mathbf{V}q)\}, \tag{1}$$

where E is evaporation, q specific humidity, \mathbf{V} horizontal velocity, and $\{ \}$ indicates a vertical integral over the entire atmospheric column. For the SCYC experiments, Eq. 1 is satisfied within each of the post- and pre-1976 runs for the annual mean. For the Jan–May period to be analyzed, a small contribution from the tendency term ($\partial q/\partial t$), essentially the difference between the end points, ($q_{\text{May}} - q_{\text{Jan}}$), remains. This term is ignored in later discussions as will be justified shortly.

Fig. 4 Various terms in the Jan–May moisture budget for the “post- minus pre-1976” difference from the SCYC runs. **a** Vertically integrated total moisture convergence. **b** Evaporation. **c** Contribution to **a** from the convergence of the product of monthly mean wind and monthly mean specific humidity. **d** Contribution to **a** from the sub-monthly moisture flux convergence. Units in mm/day with color scheme indicated at bottom

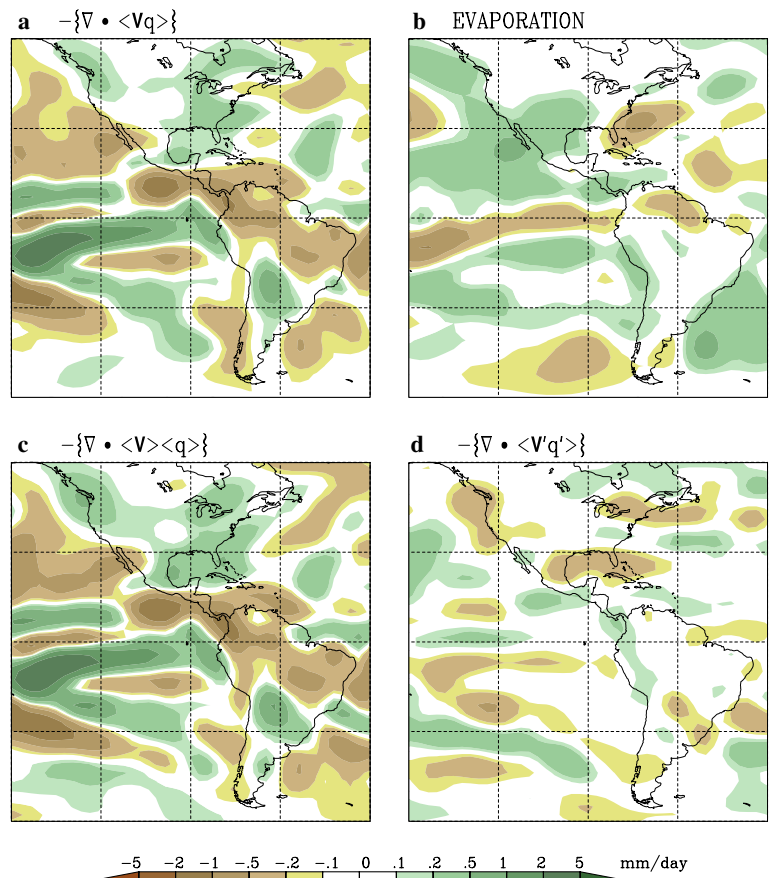
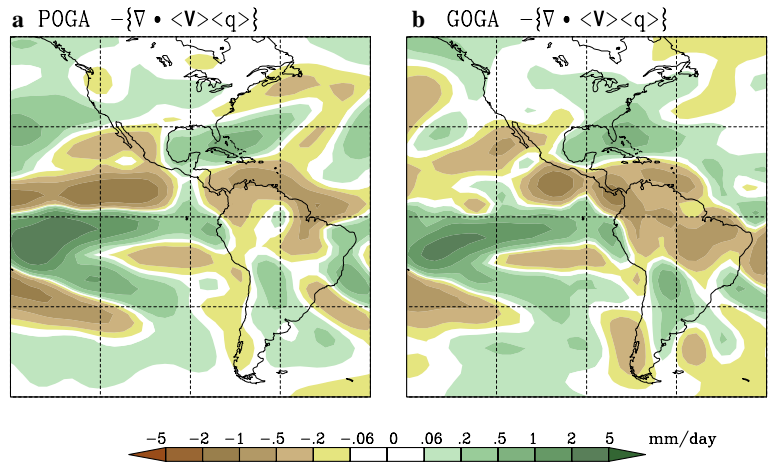


Fig. 5 Same as Fig. 4c but for a the ensemble mean of the POGA-ML runs. **b** The ensemble mean of the GOGA experiments. Units in mm/day with *color scales* indicated at bottom



Denoting the difference between the post- and pre-1976 epoch means of a variable X as

$$\delta X \equiv X_{C, \text{POST76}} - X_{C, \text{PRE76}}, \quad (2)$$

where X_C indicates the mean of the post- or pre-1976 period, the shift in precipitation across the 1976 transition can be related to those in the other terms in the moisture budget by

$$\delta P = \delta E - \delta\{\nabla \bullet (\mathbf{V}q)\}. \quad (3)$$

Here, an increase in local precipitation could be explained by an intensified moisture convergence or an increase in local evaporation. This distinction may provide useful clues to the relative importance of different dynamical/thermodynamical processes pertinent to δP .

The terms $-\delta\{\nabla \bullet (\mathbf{V}q)\}$ and δE from the SCYC runs for Jan–May are shown in Fig. 4a and b. Over Mexico and the southwest U.S., the increase in precipitation is partly balanced by an increase in evaporation, implying an intensification of local moisture recycling. Elsewhere, the δP (see Fig. 2d) is balanced mainly by moisture convergence/divergence, $-\delta\{\nabla \bullet (\mathbf{V}q)\}$. The change in moisture convergence is also important over Mexico and the southwest U.S. The δE shown in Fig. 4b is directly computed from the model output of latent heat fluxes. However, one obtains an almost identical δE if it is diagnosed from Eq. 3, another indication that the ignored term in Eq. 3, $\delta(q_{\text{May}} - q_{\text{Jan}})$, is small. (Taking the difference between the two estimates of δE as a measure of the tendency term, the variance of the latter is less than 10% of that of δE itself.) Note that this term is nonzero only if there is a shift in the annual cycle of precipitation. That it is small indicates that a shift in the seasonal cycle is not the major cause for the interdecadal shift in Jan–May precipitation.

The moisture convergence shown in Fig. 4a is the total, with contributions from sub-monthly and monthly to longer time scales. In the SCYC experiments, the total moisture flux $\mathbf{V}q$ is saved monthly (as the monthly

mean), along with the monthly means of \mathbf{V} and q . Denoting the monthly mean and the “departure from monthly mean” of a variable X as $\langle X \rangle$ and X' , the total moisture flux convergence can be decomposed into

$$-\nabla \bullet \langle \mathbf{V}q \rangle = -\nabla \bullet (\langle \mathbf{V} \rangle \langle q \rangle) - \nabla \bullet (\langle \mathbf{V}q' \rangle), \quad (4)$$

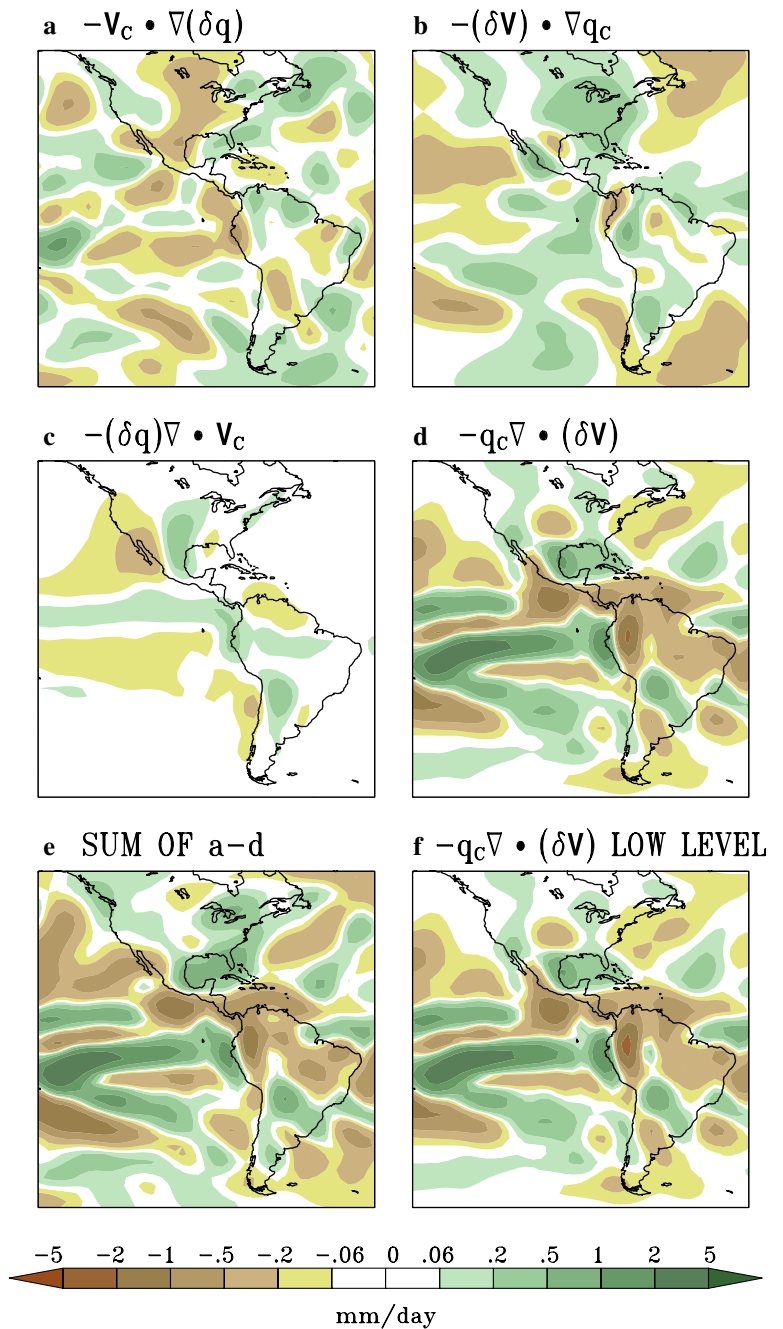
with the last term being the contribution from the sub-monthly processes that can be diagnosed from the other two. Figure 4c and d shows the post- minus pre-1976 differences in the two terms in the r.h.s. of Eq. 4. The sub-monthly term is much smaller over land and over most of the ocean. Hereafter, we will focus on the dominant term, $-\nabla \bullet (\langle \mathbf{V} \rangle \langle q \rangle)$. To completely exclude the contribution from interannual variability, we will again consider the SCYC case, but note that the differences in $-\nabla \bullet (\langle \mathbf{V} \rangle \langle q \rangle)$ across the 1976 transition simulated by the POGA-ML and GOGA runs, shown in Fig. 5a and b, are similar to that obtained by the SCYC experiments.

Detail of the shift in moisture convergence

The interdecadal shift in moisture convergence could be due to changes in the domain-averaged moisture concentration, moisture gradient, total (advective) wind, or the wind divergence. Separating these possibilities would provide additional clues to the connection between the local moisture budget and large-scale circulation. For conciseness, in the following the angled bracket $\langle \rangle$ will be eliminated, with all the \mathbf{V} and q understood as monthly means. The symbol for vertical integral, $\{ \}$ is also eliminated but is implied. A quadratic term written as XY here is equivalent to $\{ \langle X \rangle \langle Y \rangle \}$ in the preceding sections. The post- minus pre-1976 difference in moisture convergence can be rewritten as

$$-\delta \nabla \bullet (\mathbf{V}q) = \underbrace{-\delta(\mathbf{V} \bullet \nabla q)}_{(A)} \underbrace{\delta(q \nabla \bullet \mathbf{V})}_{(B)}, \quad (5)$$

Fig. 6 The major terms in the decomposition of the “post-minus pre-1976” difference in the Jan–May vertically integrated moisture convergence in Eq. (6), from the SCYC experiment. **a** Term (A1). **b** Term (A2). **c** Term (B1). **d** Term (B2). **e** Sum of **a–d**. The vertical integrals for **a–d** are for the entire atmospheric column. **(f)** Same as **(d)** but with only the lowest five levels retained in the vertical integral. Units in mm/day, with color scales indicated at bottom

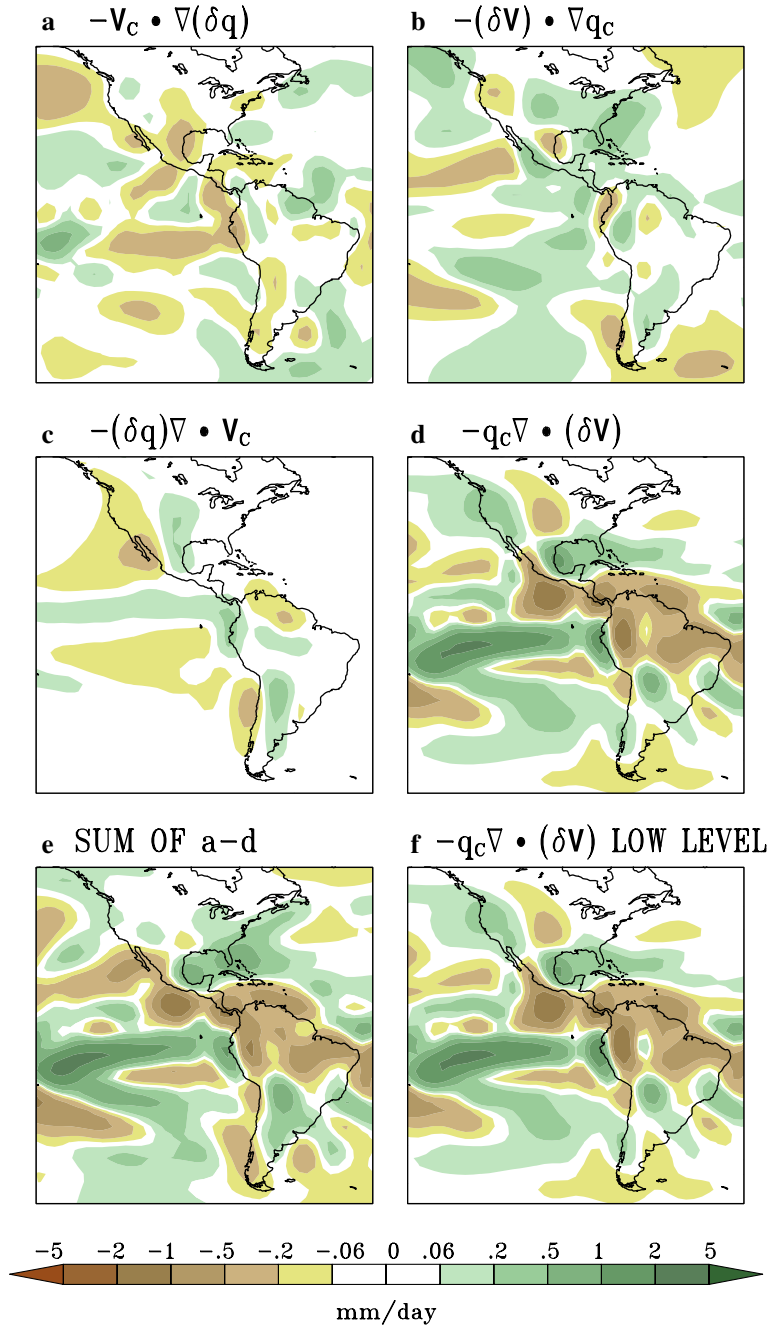


$$-\delta \nabla \cdot (\mathbf{V}q) = \underbrace{-V_c \cdot \nabla(\delta q)}_{(A1)} + \underbrace{-(\delta V) \cdot \nabla q_c}_{(A2)} + \underbrace{-(\delta q) \nabla \cdot V_c}_{(B1)} + \underbrace{-q_c \nabla \cdot (\delta V)}_{(B2)} + \text{higher order terms} \quad (6)$$

where δX and X_C are the “post- minus pre-1976” difference and the pre-1976 epoch mean of X . The expansion in Eq. 6 is intuitive but a more rigorous derivation can be found in [Appendix 3](#). The higher-order terms in Eq. 6 include quadratic terms of “ $\delta X \delta Y$ ” type and the contribution from interannual variability within the post- and pre-1976 periods ([Appendix 3](#)). The latter can be conveniently ignored as it is small for the SCYC runs.

Equations 5 and 6 provide a useful decomposition of the interdecadal shift in the total moisture convergence. Term (A) represents the effect of moisture convergence due to advection across the moisture gradient. In this case, the wind vector \mathbf{V} includes both rotational and divergent components but a further decomposition (not shown) indicates that the contribution of the rotational wind is significant. Term (B) represents the effect of wind divergence/convergence. The wind vector that is relevant

Fig. 7 Same as Fig. 6 but for the ensemble mean of the GOGA runs

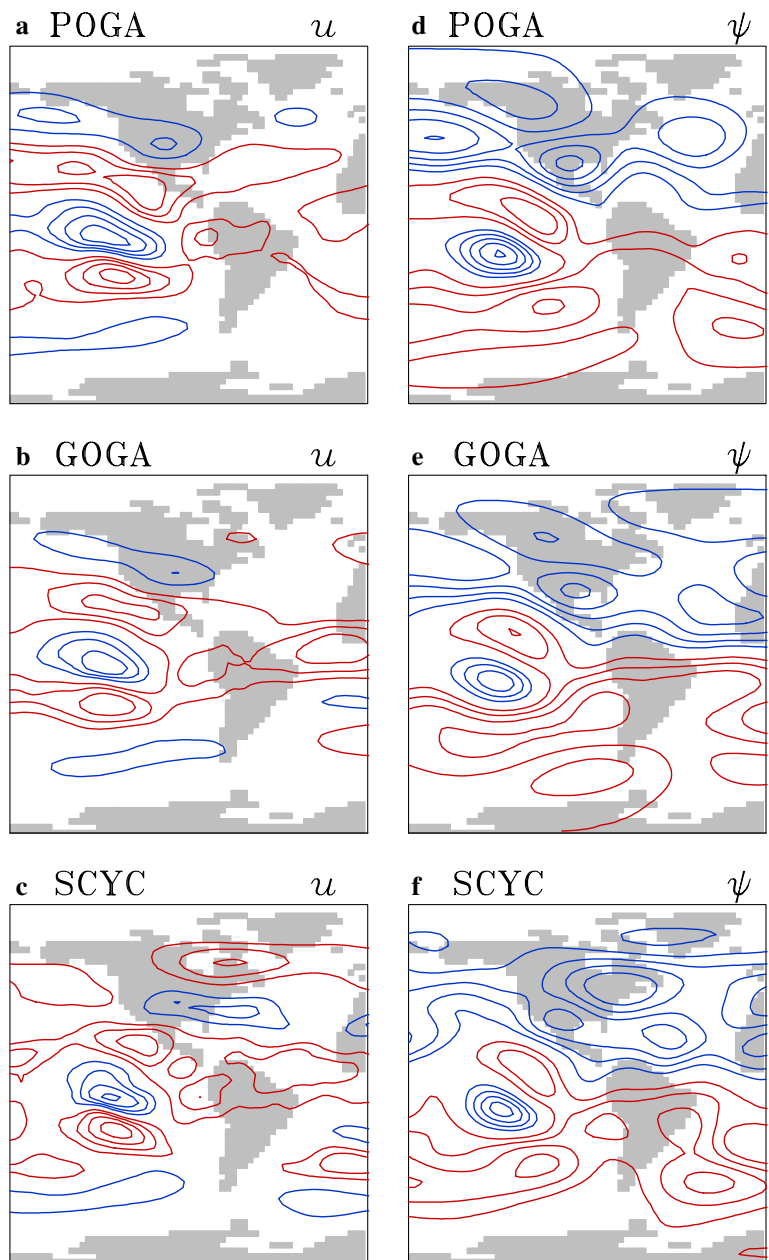


to term (B) is its divergent component. Further, the sub-term (A1) in Eq. 6 represents the effect of the changes in moisture gradient when the total advective (rotational plus divergent) wind field is fixed. Term (A2) represents the contribution from the changes in total wind field with the moisture gradient fixed. Term (B1) represents the effect of the changes in the domain-averaged moisture with a fixed divergent wind, and term (B2) the effect of the changes in the wind divergence with fixed moisture. Terms (A1)–(B2) are shown in Fig. 6a–d (remember that they are the vertical integrals). In South America and much of the Caribbean and Central America, term (B2) dominates such that the sum of the

four terms, shown in Fig. 6e, is almost identical to Fig. 6d. (That Fig. 6e resembles Fig. 4c reassures us that the higher-order terms in Eq. 6 are indeed small.) Thus, for these regions, the interdecadal shift in the total moisture convergence is due to the changes in the divergent component of the wind.

Given the dramatic decrease in specific humidity with height, the column-integrated moisture convergence in Fig. 6a–d comes mainly from the lowest few levels. This is illustrated in Fig. 6f, the same term as in Fig. 6d but with only the lowest five levels in the model (correspond approximately to 1,000–750 hPa over a flat surface) retained in the vertical integral. Clearly, the

Fig. 8 The “post- minus pre-1976” difference in the Jan–May 200 hPa zonal wind for **a** POGA-ML; **b** GOGA; **c** SCYC experiments. **d–f** are the same as **a–c** but for the 200-hPa streamfunction. Contour interval 1 m s^{-1} for zonal wind, $1 \times 10^6 \text{ m}^2 \text{ s}^{-1}$ for streamfunction. Positive and negative contours are in *red* and *blue*, with zero contours omitted



decrease in precipitation over the Amazon is balanced by a decrease in low-level wind convergence, corresponding to a weakening of the climatological ascent over this region. The closeness of Fig. 6d and f also extends to other terms (not shown) in Eq. 6, such that our previous discussion of the moisture and winds can be replaced by that of the low-level moisture and low-level winds.

Figure 7 shows the counterpart of Fig. 6 for the GOGA runs. Just like precipitation, the GOGA and SCYC runs produce similar patterns for the individual terms in the moisture budget. The POGA-ML runs also produce similar results for moisture budget but are not shown for brevity. Again, the dominant term is (B2) in Eq. 6, due to the changes in low-level wind divergence.

By mass continuity, the low-level divergence and convergence are related to descent and ascent in the lower to middle troposphere.

Over Mexico and the southwest U.S., the four terms in Eq. 6 have comparable amplitudes but their sum is not large. As already shown in Fig. 4, in this region the increase in precipitation is balanced mainly by an increase in evaporation. Over land, the changes in evaporation involve complicated processes related to soil moisture. Over the mountainous region in the southwest U.S., the Jan–May evaporation also depends on the melting of snow accumulated in the preceding fall and early winter. The change in moisture convergence remains important but clearly the interdecadal shift involves a complex interaction between the remotely

forced changes in atmospheric circulation and the local ground hydrology.

Over the northeast U.S. and Great Lakes region, the simulated interdecadal shift in precipitation is balanced by moisture convergence, although the fact that all of the sub-terms in Eq. 6, except (B1), and the sub-monthly moisture convergence (Fig. 4d) have about equal and non-negligible amplitudes renders a clear interpretation of the interdecadal pattern difficult. Note that this is also the region with a notable discrepancy between the observed and simulated interdecadal shift in precipitation, with the latter wetter than the former.

The decomposition of moisture transport in Eqs. 4, 5, 6 is useful for analyzing not only interdecadal variability but also climate changes on longer time scales. It is worth noting that, in a simple model study, Chou and Neelin (2004) found that the change in precipitation over land caused by doubled CO₂ is balanced mainly by the local moisture transport due to changes in mass divergence, a term analogous to (B2) in our Eq. 6.

5 Upper-level circulation

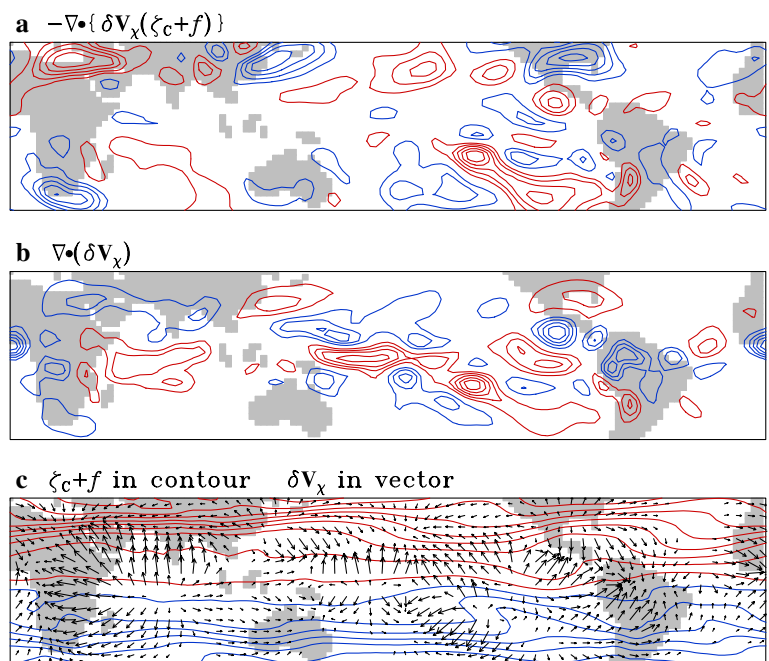
Although the interdecadal changes in precipitation over the Americas are more intimately related to low-level convergence/divergence or ascent/descent, for completeness we will present some results for the upper-level circulation, useful for a subsequent discussion on interannual and interdecadal variability. Figure 8a–c shows the post- minus pre-1976 differences in the 200 hPa zonal wind from the POGA-ML, GOGA, and SCYC experiments. A hemispherically symmetric and zonally elongated pattern, with an acceleration of subtropical jets in both hemispheres, can be readily identified in

Fig. 8a and b. This pattern is similar to the typical zonal wind response to El Niño (e.g., Seager et al. 2003; Lau et al. 2005). Since the POGA-ML and GOGA runs include the rectified effect of interannual variability, the fact that there are more strong El Niños (La Niñas) in the post- (pre-) 1976 epoch might contribute to the structures in Fig. 8a and b. However, this pattern is also present (but somewhat weakened) in Fig. 8c for the SCYC runs forced by the interdecadal SST anomaly. This indicates that the zonal wind response is not sensitive to the detail of tropical SST anomalies, a point that will be revisited in Sec. 6.

The post- minus pre-1976 differences in the 200 hPa streamfunction for the POGA-ML, GOGA, and SCYC runs are shown in Fig. 8d–f. Streamfunction, instead of geopotential height, is used here to enhance structures in the tropics. (See e.g., Hsu and Lin 1992, for a discussion of global teleconnections based on streamfunction. Since the anomalous geopotential and streamfunction are approximately related by $\delta\Phi \sim f\delta\psi$, where f is the Coriolis parameter, in the lower latitudes the geopotential height anomaly is flatter.) In the streamfunction field, a pair of Rossby wave trains emanating from the tropical Pacific to the midlatitudes of both hemispheres are more clearly seen as responses to the tropical SST anomalies (e.g., Trenberth et al. 1998). These wave trains are not significantly different among the SCYC and POGA-ML/GOGA runs.

Notably, even with its maximum located south of the equator, the interdecadal SST anomaly (Fig. 1c) produces a cross-equatorial wave train that propagates into the Northern Hemisphere. This can be understood in two ways: first, in boreal winter the longitudinal sector on the equator from 150°W–90°W is predominantly westerly, allowing a pathway for cross-equatorial wave

Fig. 9 **a** One of the components of the anomalous (post- minus pre-1976) Rossby wave source, $-\nabla \cdot \{\delta \mathbf{V}_x(\zeta_c + f)\}$, at 200 hPa for Jan–May. **b** Post- minus pre-1976 divergence at 200 hPa. **c** Contours of the 200-hPa climatological absolute vorticity superimposed with vectors of the divergent component of horizontal wind corresponding to the anomalous divergence in Fig. 9b. All three panels are from the ensemble average of GOGA runs. Contour interval is arbitrary for **a** and **b**, and 0.2Ω (where Ω is the rotation rate of the Earth) for **c**. Blue is negative for all panels. Zero contours are suppressed for **a** and **b** but retained for **c** to show the dynamical equator



propagation (Webster and Holton 1982; Hsu and Lin 1992). Second, the Rossby wave source (RWS, Sardeshmukh and Hoskins 1988) responsible for the generation of upper-level Rossby waves can spread beyond the confines of the SST anomaly itself (see Sardeshmukh and Hoskins 1988). In our problem, the post- minus pre-1976 difference in RWS, δRWS , can be produced by both positive and negative divergence anomalies associated with anomalous precipitation (Fig. 2c). To illustrate, Fig. 9a shows one of the major components of δRWS , $\delta RWS_1 = -\nabla \cdot \{\delta \mathbf{V}_\chi(\zeta_C + f)\}$, due to the anomalous divergence acting on the climatological absolute vorticity at 200 hPa for Jan–May from the ensemble mean of the GOGA runs. (As usual, δX and X_C represent the post- minus pre-1976 difference and the pre-1976 epoch mean of X . \mathbf{V}_χ , ζ , and f are the divergent components of horizontal wind vector, relative vorticity, and the Coriolis parameter.)

In the tropics δRWS_1 is concentrated over the eastern Pacific, supporting our argument that the anomalous Rossby wave trains shown in Fig. 8 originate from this region. (In Fig. 9a, a few centers of δRWS_1 also exist in midlatitude. They are partly related to jet exits and entrances (e.g., Nakamura 1993; Robinson 1994) and might play a role in exciting midlatitude Rossby waves (e.g., Qin and Robinson 1993). An analysis of this part of δRWS is more complicated and is left for future work.)

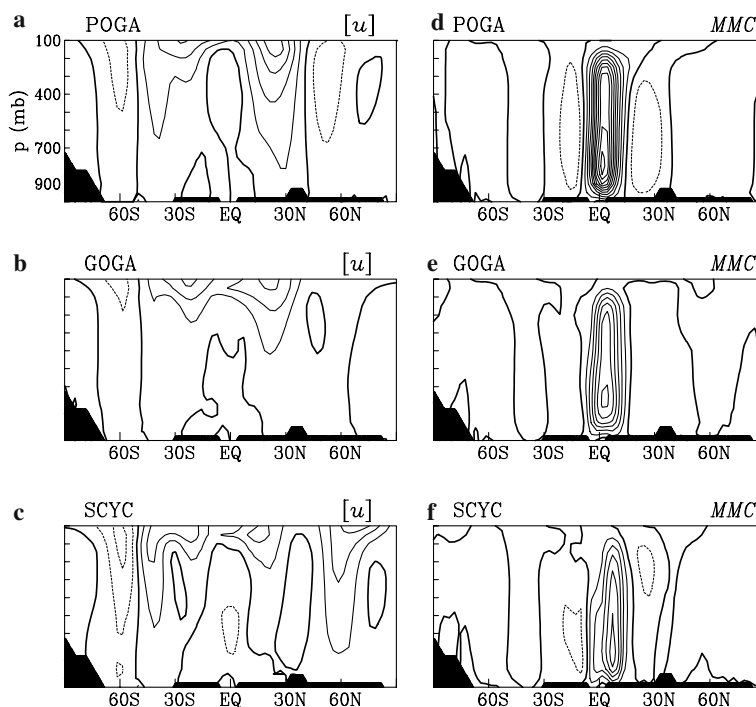
It is worth noting that, although the post- minus pre-1976 200 hPa divergence, shown in Fig. 9b, exhibits two strong positive centers over the equatorial western Pacific and Indian Ocean (related to the positive SSTAs there in Fig. 1c), the corresponding δRWS_1 is not large

there. This is because the meridional gradient of absolute vorticity over the western Pacific and Indian Ocean is not as tight as that over the eastern equatorial Pacific, as shown in Fig. 9c. This explains the smallness (compared to eastern Pacific) of one of the sub-components of δRWS_1 , $-\delta \mathbf{V}_\chi \cdot \nabla(\zeta_C + f)$, over the former two regions. The other sub-component, $-(\zeta_C + f)\nabla \cdot (\delta \mathbf{V}_\chi)$, is also not large over those regions because the centers of anomalous divergence there nearly coincide with the dynamical equator, the contour of $\zeta_C + f = 0$, as shown in Fig. 9c.

In Fig. 8, the anomalous wave trains are located mostly over the ocean but they intersect with the American continents with a low over Mexico and the southwest U.S. and a trough over the southern tip of South America. Although it is tempting to relate these two features to the wet and dry anomalies in precipitation in these two regions, we instead caution that, in general, upper-level highs/lows and precipitation do not have a simple one-to-one correspondence (see e.g., Bates et al. 2001 for examples showing the disparity of this relationship) since the latter depends on additional factors such as large-scale moisture supply, local topographic lifting, etc.

Although the recently constructed “reanalysis” data sets include grided upper-level winds for the pre-1976 period, their reliability depends on the density of upper-air observations that can be scarce especially over the oceans. A quick look at the post- minus pre-1976 difference in the NCEP/NCAR reanalysis reveals no clear patterns of the wave train over the southeast Pacific shown in Fig. 8d–f. However, records also indicate that there is virtually no coverage of upper-air observations in this region for the pre-1976 period (see Fig. 5.3 of

Fig. 10 The “post- minus pre-1976” difference in the Jan–May zonal mean zonal wind for **a** POGA–ML; **b** GOGA; **c** SCYC experiments. **d–f** are the same as **a–c** but for the mean meridional circulation (MMC) represented by the Stokes streamfunction in meridional plane (Peixoto and Oort 1992, chap. 7). Contour interval 0.5 m s^{-1} for zonal mean zonal wind, $2.5 \times 10^9 \text{ kg s}^{-1}$ for MMC. Negative contours are *dashed*, and zero contours *bold solid*. The positive contours in **d–f** correspond to clockwise circulation in the meridional plane. The maxima on the maps in **d**, **e**, and **f** are 26.2 , 15.5 , and $14.0 \times 10^9 \text{ kg s}^{-1}$



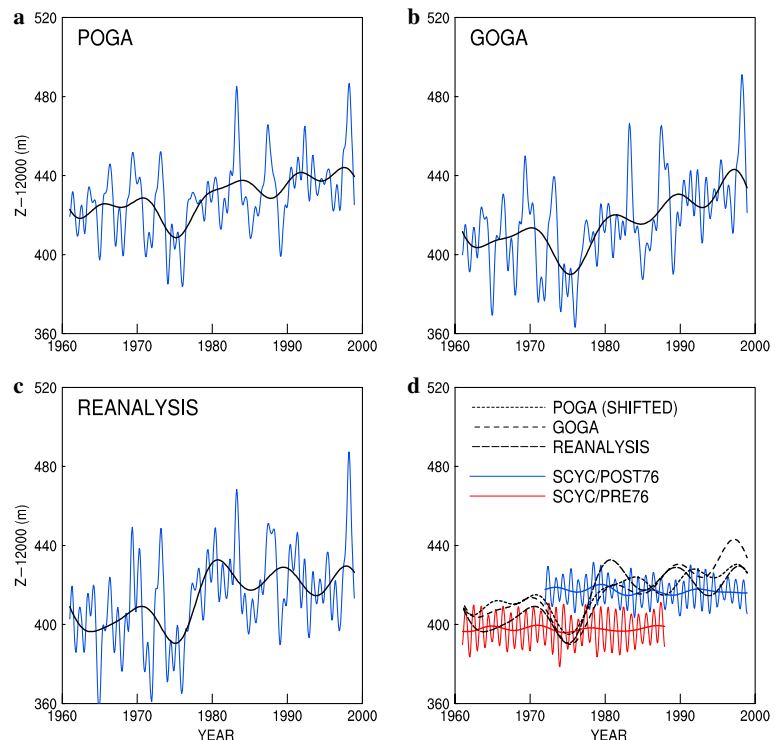
Peixoto and Oort 1992). (For further discussions on the limitations of the tropical circulation in reanalysis, see Trenberth et al. 2001; Kinter et al. 2004.) To avoid misinterpretations, we choose not to rely on the reanalysis data to verify the simulated interdecadal shift in the upper-level circulation.

Figure 10a–c shows the post- minus pre-1976 difference in the zonal mean zonal wind from the POGA-ML, GOGA, and SCYC runs. A common feature of the three panels is the acceleration of subtropical jets at the upper troposphere in both hemispheres. This structure is accompanied by a zonally symmetric, tropics-wide increase of tropospheric temperature (see Sect. 6 and Figs. 11, 12). Again, the results for SCYC are not dramatically different from POGA-ML/GOGA. (The difference between Figs. 10c and 10a and b in the higher latitudes in Northern Hemisphere could be due to the difference in sea ice in the boundary forcing (see Appendix 1) or other dynamical processes related to wave-zonal mean interaction in high latitudes.) Notably, all three types of runs produce a deceleration of westerly zonal wind at 60°S, opposite to that in the reanalysis (e.g., Thompson et al. 2000). Keeping in mind our previous caution about reanalysis in the pre-1976 era, this difference might otherwise be related to the trends in sea ice and greenhouse gas concentration. The former is treated very crudely in our GCM runs due to the lack of observations for the early years (Appendix 1). The trend in greenhouse gas concentration is not explicitly included in our simulations, but note that part of the greenhouse-gas effect is embedded in the SST. In the lower latitudes, the post- minus pre-1976 difference in Jan–May zonal mean zonal wind in NCEP/NCAR

reanalysis (not shown) does not exhibit a hemispherically symmetric pattern of acceleration of the subtropical jets simulated by the GCM. Instead, the acceleration is centered almost at the equator with its maximum in the lower stratosphere (for useful references see Fig. 4 of Abarca del Rio 1999; Fig. 9 of Schneider et al. 2003). This positive center is flanked by easterly anomalies in the subtropics, with the deceleration in the Southern Hemisphere more pronounced than in the Northern Hemisphere. These differences between GCM simulations and reanalysis remain to be explained.

The divergent wind response to tropical SST forcing has a zonally symmetric component that has been shown to provide a major contribution to the midlatitude moisture budget during El Niño (Seager et al. 2005). The zonal mean low-level divergence/convergence is associated with the descent/ascent of the mean meridional circulation (MMC). Figure 10d–f is the same as Fig. 10a–c but for the MMC. The most robust feature in Fig. 10d–f is a single tropical cell with its rising branch located slightly south of the equator, consistent with the slightly south of the equator maximum in the interdecadal SST pattern in Fig. 1c. The counterpart of Fig. 10d–f for the NCEP/NCAR reanalysis (not shown) exhibits a similarly oriented single-cell structure in the tropics with a comparable magnitude and with its rising branch located in the Southern Hemisphere. The meridional extent of that cell is slightly wider than those simulated by the GCM. In general, the simulated MMC resembles that in the reanalysis more closely than zonal mean zonal wind. Away from the tropics, the zonal mean MMC in the model is due to contributions from different longitudinal sectors that is not easy to interpret.

Fig. 11 The tropical (20°S–20°N) average of 200 hPa height, shown as the departure from 12000 m. **a** The ensemble mean of POGA-ML runs. *Blue line* shows the 9-month low-pass-filtered time series, *bold black line* the decadal-to-interdecadal component obtained by a Fourier analysis. **b** Same as (a) but for GOGA runs. **c** Same as (a) but for the NCEP/NCAR reanalysis. **d** The three black curves from a–c are redrawn as dashed curves, with a slight shift of the POGA curve to compensate a bias (see text). The 9-month low-pass-filtered time series (*thin*) and decadal/interdecadal components (*bold*) of the post- and pre-1976 SCYC runs are shown in *blue* and *red*, respectively



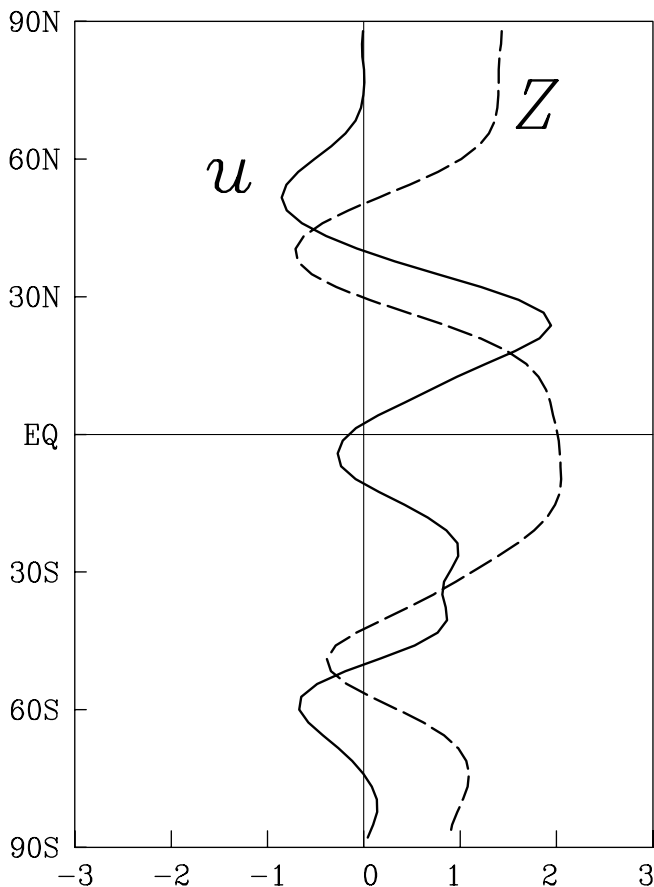


Fig. 12 The meridional profiles of the post- minus pre-1976 differences in 200-hPa zonal mean geopotential height (*dashed*) and zonal mean zonal wind (*solid*) from the POGA runs. Units are 1 m s^{-1} for zonal wind, 10 m for height

A quick estimate (not shown) reveals that, in midlatitude, the simulated low-level zonal mean divergence/convergence is a relatively small residue of the local divergence/convergence pertinent to the moisture convergence over land discussed in Sect. 4. The zonal mean divergence is only one component of the interdecadal shift in local precipitation and moisture budget over the Americas.

6 Further remarks on interannual and interdecadal variability

In the eastern Pacific, the major difference between the interdecadal and interannual (El Niño) SST anomalies is that the maximum of the former is located south of the equator. Despite this difference, we have shown that the responses in atmospheric circulation and precipitation over the Americas to these two SST patterns are not dramatically different. Seeking an explanation for this similarity, we first note that during El Niño the air temperature anomaly induced by the local SST anomaly in the equatorial Pacific spreads in the longitudinal direction, such that within one to two seasons the entire

tropics have the same sign of tropospheric temperature anomaly (Yulaeva and Wallace 1994; Chiang and Sobel 2002). This leads to zonally and hemispherically symmetric temperature gradients in the subtropics in both hemispheres that are pertinent to the zonally and hemispherically symmetric zonal wind signals in the subtropics and, through a secondary process involving the eddies, the extratropics (Seager et al. 2003). The east–west homogenization of air temperature occurs in the vicinity of the equator because, due to the smallness of the Coriolis parameter, there are no dynamical terms to balance a longitudinal pressure gradient (Charney 1963). Any imbalance is likely removed by the equatorial Kelvin waves through an eastward spreading of the temperature anomaly (see Chiang and Sobel 2002 for such a sequence following El Niño). The tropical zone of homogenized temperature is very broad, extending to about 20°N and 20°S (Chiang and Sobel 2002). As such, any SST anomaly, regardless of its detailed shape and location, that falls within this zone may produce a similar end state with the homogenized temperature. Extending this argument to the interdecadal SST pattern in Fig. 1c, one would expect similar thermodynamical responses in the tropical troposphere to the interdecadal and interannual SST anomalies.

Before proceeding further, we should now verify that the POGA-ML, GOGA, and SCYC runs produce comparable interdecadal (upward) shifts in the tropics-wide tropospheric temperature across the 1976 transition. The 200 hPa height averaged over the tropics (20°S – 20°N) is used as an index for tropical tropospheric temperature. (The 200 hPa level is lifted when the troposphere expands due to an increased temperature.) Figure 11a–c shows this index, denoted as Z_{200} , for 1961–1998 from the POGA-ML and GOGA runs and the NCEP/NCAR reanalysis. The thin blue lines are the 9-month low-pass filtered time series of Z_{200} , shown as its departure from 12,000 m, and bold black lines the decadal-to-interdecadal component consisting of only the variability with $T > 6$ years. Although the annual cycle is retained in the blue lines in Fig. 11a–c, it is overwhelmed by interannual variability. For example, the four highest peaks in the blue line in Fig. 11a are due to the 1982/83, 1986/87, 1992/93, and 1997/98 El Niños. They contribute to the higher epoch mean of Z_{200} in the post-1976 period. The decadal-to-interdecadal components in Fig. 11a–c are very similar, all showing an upward trend for the second half of the twentieth century but with the 1976 shift more pronounced in the reanalysis (see also Seager et al. 2004). The three black curves in Fig. 11a–c are re-plotted in Fig. 11d as the dashed curves. Because the Z_{200} for POGA-ML is systematically higher than GOGA (by about 13 m, a small bias considering that the total 200 hPa height is over 12,000 m), the POGA-ML case in Fig. 11d is shifted for the purpose of demonstration. All three dashed curves in Fig. 11d show a clear elevation of Z_{200} in the post-1976 era. Also shown in Fig. 11d are the post-1976 (blue) and pre-1976 (red) SCYC runs, presented in the same format

as Fig. 11a–c. The 9-month low-pass filtered time series (thin lines) for the SCYC runs are dominated by the annual cycle, with only weak and random interannual and decadal variability. Nevertheless, because the tropical mean SST is higher in the post-1976 period, it elevates the epoch mean of Z_{200} for this period, resulting in a post- minus pre-1976 difference in Z_{200} comparable to those obtained from POGA-ML, GOGA, and reanalysis. The meridional profiles of the post- minus pre-1976 zonal mean 200 hPa geopotential height and zonal wind for POGA-ML runs are shown in Fig. 12. The tropical warming zone extends to 20°–25° latitudes, where a sharp meridional temperature (or height) gradient is accompanied (noting thermal wind balance) by an enhanced subtropical jet in both hemispheres. The structure of the height anomaly in Fig. 12 is also reminiscent of those associated with multi-year droughts analyzed by Schubert et al. (2004, see their Figs. 2, 6).

By a thermodynamical control argument (Chiang and Sobel 2002 and references therein), the uniform band of warmer tropical air in the post-1976 era could induce detailed structures in tropical precipitation anomalies common to the POGA-ML, GOGA, and SCYC runs. For example, as an El Niño or interdecadal SST anomaly produces the banded warming in the tropical troposphere, warmer air would spread eastward over the Amazon, reducing the local lapse rate there. This results in a more stable atmosphere with suppressed precipitation (as in Figs. 2, 3) and anomalous descent. The weaker upward motion is in turn compensated by a reduced low-level convergence (as in Figs. 6d, 7d). (The last two steps are our own interpretation. Chiang and Sobel (2002) have focused on the thermodynamical mechanism over the ocean.) In this view, the chain of reaction starts with the change in tropospheric temperature induced by remote SST anomalies. The change in local low-level divergence or vertical motion is a passive response to the change in precipitation, which itself is an adjustment to the change in vertical thermodynamical profile. This argument is appealing as it does not depend on the detail of the SST anomalies.

Note that the effect of an increased CO_2 concentration, which might be partially responsible for the observed interdecadal changes in precipitation, is implicitly embedded in the SST in our model (in the sense that an increase in the tropical Pacific SST is simulated by many coupled GCMs with double CO_2 , as mentioned in Sect. 2). Clearly, the trend in SST alone does not represent the complete effect of the greenhouse gas forcing. If an explicit trend in CO_2 were included in our simulations, land masses would have likely warmed up more dramatically in the last 40 years. In the context of our thermodynamical argument, this would weaken the expected effect of the stabilization of the troposphere over the Amazon (as suggested to the authors by E. K. Schneider). This might explain why the simulated drying over the Amazon in Fig. 2c is more extensive than that observed in Fig. 2a.

For ENSO variability, although the zonal band of tropospheric warmth is restricted to the tropics, its existence is enough to induce a secondary response in dynamical fields (Seager et al. 2003 and references therein) and precipitation (Seager et al. 2005) in the extratropics in both hemispheres. Details aside, in this scenario the midlatitude response is controlled by the tropical tropospheric warmth. Thus, if the tropical warm bands produced by the interannual and interdecadal SST anomalies are similar, they would induce similar responses in midlatitude. Robinson (2002) and Seager et al. (2003) suggest that the secondary extratropical response is driven by the eddies that propagate differently after the modification of the large-scale wind/temperature basic states by the tropical warmth. It is worth extending their analyses to interdecadal variability in the future.

In the tropics, some differences between the simulated ENSO and interdecadal precipitation anomalies remain (compare Fig. 2c to Fig. 3b) that cannot be explained by the thermodynamical argument. Most notable in the American sector is the dryness over the Caribbean and northern tip of South America in the interdecadal pattern that is absent in the ENSO composite for the GOGA runs. This could be the region where the direct circulation response to the detailed SST anomalies matters. To test this, one would need a dynamical model for the tropics that can predict the divergent wind response to SST forcing (for example, the damped linear solution of Gill (1980) or the inviscid nonlinear solution of Schneider (1987), preferably modified to incorporate more realistic orography and vertical resolution.) The relative importance of the thermodynamical and dynamical control of SST-induced precipitation anomalies needs further investigations.

While the similarity between the simulated precipitation in GOGA and POGA-ML runs indicates the importance of tropical Pacific SSTs, it does not rule out potential contributions of the Indian Ocean SST to the interdecadal precipitation anomalies over the Americas. Because the SST anomalies in Indian and other ocean basins are influenced by the tropical Pacific SST through the “atmospheric bridge” (Alexander et al. 2001), it might be more difficult to isolate their effects with POGA-ML type experiments. Within the Pacific basin, there are interesting features in the interdecadal SST patterns in Fig. 1, notably the hot (or cold) spot off the coast of Mexico, which have not been emphasized in this work. As this hot spot is represented by a very small number of grid points due to the moderate T42 resolution of CCM3.10, simulations with a high-resolution regional model may be more suitable for clarifying the impact of this SST anomaly pattern on regional precipitation.

The similarity between the precipitation in SCYC and GOGA/POGA-ML runs indicates that the rectified effect of interannual variability is not crucial for producing the interdecadal shift in precipitation over the Americas. This is understood in the sense that one does

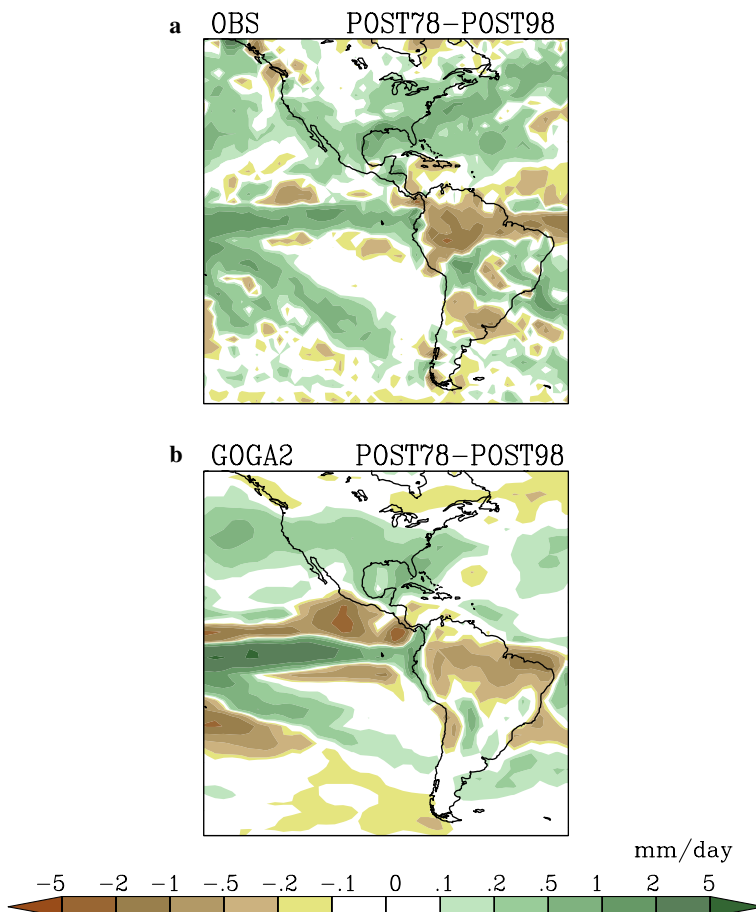
not need to accumulate the responses in precipitation to individual El Niños/La Niñas in order to recover the interdecadal anomalies in precipitation. In other words, the rectified effect arising from the nonlinear relationship between SST and midlatitude precipitation is unimportant. To the first order, the interdecadal precipitation anomalies are linear responses to the interdecadal modulation of tropical SSTs. The latter, which is reflected in the difference between the post- and pre-1976 mean seasonal cycles of SST in the SCYC runs, could be due to the various causes—global warming, internal atmosphere–ocean dynamics, and changes in the characteristics of El Niño—cited in the Introduction. Our conclusions are restricted to the precipitation responses to given SSTs and do not endorse or reject any of these scenarios regarding the origins of the interdecadal SST patterns.

7 A 1998 reversal?

We have chosen the middle of 1998 as the end point of the post-1976 period, based on recent observations that suggest a reversal of the post-1976 trend in the precipitation over several regions of the Americas, notably the occurrence of the 1998-present North American drought (Hoerling and Kumar 2003). Comparing

Fig. 13a, the observed “post-1976 minus post-1998” difference in the Jan–May precipitation, to the “post-1976 minus pre-1976” picture in Fig. 2a, one finds similarities in the southwest U.S. and northern half of South America but also differences elsewhere. (Here, the post-1998 period is defined as July 1998–June 2003. The NOAA/CPC CMAP data set, which incorporated Satellite observations, is used for Fig. 13a. It was not used in Sect. 4 as it starts in 1979. Without 1976–1978 in the CMAP data, the “post-1976” period shown in Fig. 13 is actually “post-1978” but the minor difference is inconsequential.) It is interesting to compare the simulated changes in precipitation across the two turning points at 1976 and 1998. For this purpose, a smaller set of 16 ensemble members of the GOGA runs (marked in Fig. 13 as “GOGA2”) are extended to 2004. The model reproduced the “post-1976 minus post-1998” differences in precipitation over Mexico and the southwest U.S. and the northern half of South America, as shown in Fig. 13b. The Jan–May SST anomaly, defined as the departure from the 1871–1999 mean, for the post-1998 period is shown in Fig. 14. It is quite different from the pre-1976 picture in Fig. 2b. The equatorial Pacific has cooled but the rest of the Indo-Pacific Oceans remains warm. In addition, the cold anomaly is centered on the equator, in the middle of the basin. (Hoerling and Kumar 2003 suggest that

Fig. 13 The “post-1976 minus post-1998” difference in the Jan–May precipitation for **a** observation based on the CMAP data set. **b** Ensemble mean of 16 GOGA runs. *Color scales* are indicated at the bottom



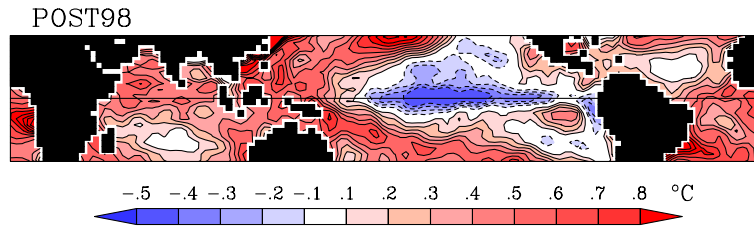


Fig. 14 The Jan–May SST anomaly, defined as the departure from the 1871–1999 mean, for the post-1998 period. Contour interval 0.1°C, negative dashed. Areas with the absolute value of SST anomaly greater than 0.1°C are filled with *red* (positive) and *blue* (negative) colors

this unique SST pattern is responsible for producing the 1998–2002 North American drought.) With this limited evidence, we suggest that the post-1976 “warm phase” (characterized by the SST pattern in Fig. 1a) has ended but a new “cold phase” of an interdecadal oscillation has not yet been fully established.

8 Conclusions

Most major features of the interdecadal shift in boreal winter–spring precipitation over the American continents across the 1976 transition are reproduced in atmospheric GCM simulations forced with observed SST. The POGA-ML runs forced with specified tropical Pacific SST produce similar results as the GOGA runs with global SST, indicating the importance of tropical Pacific SST in forcing interdecadal variability in precipitation over the Americas. Two types of simulations with the forcing including (GOGA) and excluding (SCYC) interannual variability of tropical Pacific SST also produce similar interdecadal shifts in the upper-level circulation and precipitation over land in the American sector. This indicates that the precipitation shifts arise fundamentally from shifts in the mean tropical climate rather than as a rectified effect due to the nonlinear relationship between SST and precipitation. In fact, the observed and simulated interdecadal shifts in Jan–May precipitation—wet over Mexico and the southwest U.S., dry over the Amazon, wet over sub-Amazonian South America, and dry over the southern tip of South America—are not dramatically different from a typical El Niño-induced response in precipitation. This implies that the responses in atmospheric circulation and precipitation over the Americas are not sensitive to the detailed differences between the El Niño and interdecadal SST anomaly patterns, the latter having its maximum south of the equator. The “tropospheric temperature” control thinking (Chiang and Sobel 2002; Neelin et al. 2003), namely, warm tropical Pacific SST anomalies influence remote precipitation by elevating and homogenizing tropics-wide tropospheric temperature, provides a plausible explanation of this insensitivity for the responses in the tropics. The tropical tropospheric warmth common to the interannual and interdecadal atmospheric responses may, in turn, induce similar secondary responses in the extratropics through an

anomalous eddy forcing as argued by Seager et al. (2003) and Robinson (2002).

An analysis of local moisture budget shows that, except for Mexico and the southwest U.S. where the increase in precipitation after 1976 is balanced by evaporation, the shift in precipitation elsewhere over the American continents is balanced by low-level moisture convergence. Furthermore, the interdecadal shift in moisture convergence is due mainly to the change in low-level wind divergence that is linked to low-level ascent and descent. This is similar to the finding of Seager et al. (2005) for ENSO variability that the tropical SST-forced wet precipitation anomalies in midlatitudes are associated with anomalous ascent.

The two decades of dry tropics and wet midlatitudes over the Americas ended in 1998. The model results show that this latest shift was caused by the shift to cooler SSTs in the tropical Pacific, even as the Indian Ocean remained warm.

The findings in this study reinforce the emerging consensus of the tropical control of global climate, previously explored in the context of multi-year droughts (Hoerling and Kumar 2003; Schubert et al. 2004; Seager et al. 2005; manuscript submitted to *J. Climate*), hemispherically symmetric climate variability (Seager et al. 2003), and the long-term trend (Hoerling et al. 2001; Schneider et al. 2003) in observations and/or GCM simulations.

Acknowledgements The authors thank Dr. Naomi Naik for valuable help and advices on the models used in this study, Dr. Alexey Kaplan for providing up-to-date SST data sets for the GCM experiments, and the two anonymous reviewers and Dr. Edwin Schneider for useful comments. The GFDL data used in Fig. 15a was provided by GFDL’s climate modelling group. This work is supported by the NOAA CLIVAR-PACS program and NSF grant ATM 0347009, and is funded in part under the Cooperative Institute for Climate Applications and Research (CICAR) award number NA03OAR4320179 from the National Oceanic and Atmospheric Administration, U.S. Department of Commerce. This is Lamont-Doherty Earth Observatory Contribution No. 6735.

Appendix 1

Models and SST for GCM experiments

The GOGA, POGA-ML, and SCYC runs were performed for multiple purposes and executed over time in

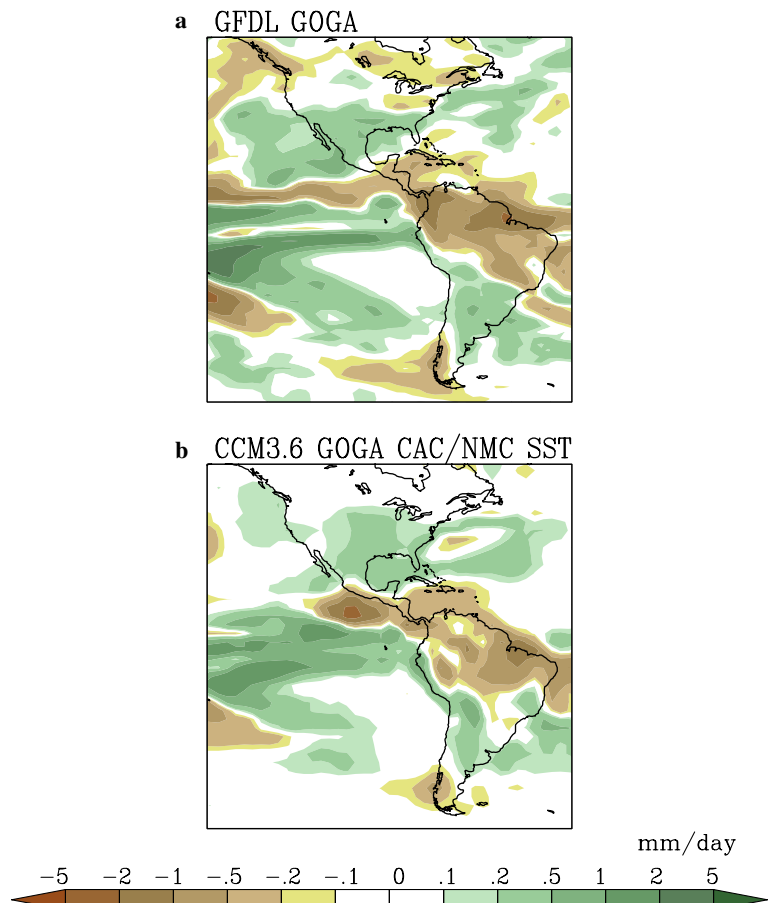
conjunction with the ongoing updates of several comprehensive SST data sets. As a result, they were not forced with exactly the same SST data set. This does not affect our conclusions, as the SST forcing for the post-1961 period considered in this work does not depend strongly on the choice of the data set. Specifically, in the GOGA experiments the atmosphere GCM uses observed SSTs in its lower boundary. These use a blend of data sets. The HadISST data set (Rayner et al. 2003) begins in 1870 and is global. The data set of Kaplan et al. (1998) begins in 1856, is not global, but does contain data in the tropics for the whole time. Therefore, for the tropical Pacific (20°N–20°S) we use Kaplan data from 1856 to 2001. From 1856 to 1870, and outside of the tropical Pacific, we use Kaplan data where available and otherwise use climatological SSTs from HadISST. From 1870 on, and outside the tropical Pacific, we use the HadISST data. The SSTs were smoothed linearly in latitude across a 10° wide belt between the tropical Pacific and the north and south Pacific Oceans. This ensures that the merger does not produce a jump discontinuity in space. A comparison of our GOGA runs with a set of similar runs forced with a single set of SST forcing (see Fig. 15b) reveals minimal differences, inconsequential to our conclusions.

For the POGA-ML experiments, we only specify the SST in the tropical Pacific, using the Kaplan data, and compute the SSTs everywhere else using an ocean mixed layer model to be described shortly. In this model, SST anomalies outside of the tropical Pacific can only be generated by surface flux variability caused by internal atmospheric variability or forced as a response to the imposed tropical Pacific variability.

The epoch-mean seasonal cycles of SST used to force the SCYC runs are constructed from the HadISST1 data set (Rayner et al. 2003). Due to the great uncertainty in sea ice in the pre-1976 era, we choose not to include the epoch difference in sea ice in the boundary forcing. A default climatological annual cycle of sea-ice distribution (constructed from 1979–1995) that came with the CCM3.10 model is used in both post- and pre-1976 runs. Thus, the difference between the two SCYC runs reflects only the impact of the open-ocean SST in the middle and lower latitudes.

In the POGA-ML runs, the atmospheric GCM is coupled to a model of the ocean mixed layer (ML) outside the tropical Pacific. The ML model is based on Russell et al. (1985) and includes a variable depth surface layer that exchanges mass and heat with a layer below that extends down to a uniform specified depth. The depth of the surface layer follows a pre-

Fig. 15 **a** The post-1976 minus pre-1976 precipitation simulated by a single GOGA run with the GFDL AM2 model. **b** Same as **a** but for the ensemble average of 12 GOGA runs with NCAR CCM3.6. See text for details



scribed seasonal cycle that is spatially variable and which follows the observed ML depth, taken to be the depth where the temperature falls more than 0.5 K cooler than the SST using the data of Levitus and Boyer (1994). The surface layer exchanges heat with the atmosphere according to the atmosphere GCM's computation of the surface energy fluxes. The surface layer exchanges heat with the subsurface layer that is derived from the specified mass exchange and the modelled layer temperatures. The movement of heat by ocean currents in each layer is specified according to the "q-flux" formulation: a spatially varying seasonal cycle of "q-flux" is diagnosed for each layer as that which is required to maintain the observed climatological model temperatures when the ocean model is coupled to the atmosphere GCM (see Russell et al. 1985 for details). The q-fluxes also account for errors in the modeled surface flux (and other model errors) but, primarily, account for the ocean heat transport.

The T42, 18-level version of NCAR CCM3.10 is adopted as the atmospheric GCM for our GOGA, POGA-ML, and SCYC experiments. Although our results are based on one model, preliminary model intercomparisons indicate that the multidecadal change in precipitation simulated by CCM3.10 (and verified with observations) is not sensitive to the model and the SST data set used for boundary forcing. Figure 15a shows the "post-1976 minus pre-1976" precipitation (to be compared with Fig. 2c) simulated by a single GOGA run with GFDL AM2 model. The wet condition over southwest U.S. and Mexico and dry condition over northern South America are reproduced. Figure 15b is similar to Fig. 15a but is the average of an ensemble of 12 GOGA runs with NCAR CCM3.6 (a close relative of CCM3.10), identical to those used in Huang et al. (2003). Here, 5 of the 12 members are forced with the Climate Analysis Center (CAC) SST data set, the other 7 with the slightly different National Meteorological Center (NMC) data set. Both CAC and NMC data sets are forerunners of the Reynolds SST data set (Smith et al. 1996), different from the Kaplan and HadISST data used in our experiments. Yet, the simulated interdecadal changes in precipitation over the Americas are very similar, confirming the insensitivity of our results to SST data set. The similarity between Figs. 2c and 15b (the latter forced by a single SST data set) also reassures us of the soundness of our approach of combining Kaplan and HadISST data in the boundary SST forcing.

simulated by the GCM. Denoting the two epoch means of precipitation for the k -th ensemble member of the GCM runs as $P_{\text{POST},k}$ and $P_{\text{PRE},k}$, we are concerned

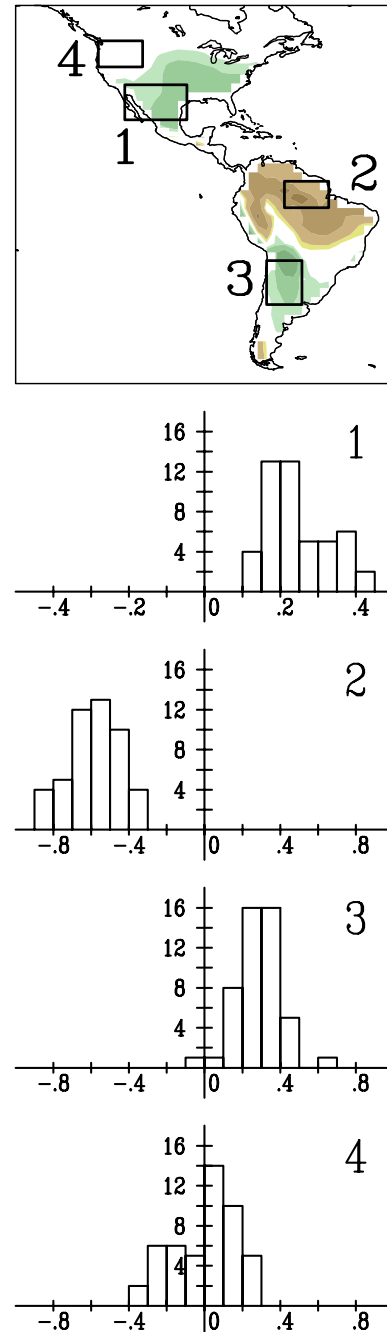


Fig. 16 The map at top panel repeats Fig. 2c but with boxes 1–4 marking the regions where the statistical significance of the post-minus pre-1976 difference in Jan–May precipitation, $\{\Delta P_k\}$, will be tested for the GOGA runs. Lower panels marked by 1–4 are the histograms of $\{\Delta P_k\}$ for the 48 ensemble members for the corresponding boxes. Units are mm/day for the abscissa and numbers of ensemble members for the ordinate. The bin widths for the histograms are 0.05 mm/day for box 1 and 0.1 mm/day for the other three boxes

Appendix 2

Statistical significance of the simulated post- minus pre-1976 difference in precipitation

The quantity of our interest is the difference between the post- and pre-1976 epoch means of precipitation

about the statistics of $\Delta P_k \equiv P_{\text{POST},k} - P_{\text{PRE},k}$. In particular, we wish to determine, given the number of independent samples (considered here as the number of ensemble members), whether the mean of $\{\Delta P_k\}$ is significantly positive or negative at the major centers of the pan-American precipitation pattern discussed in the main text. As a demonstration, the map in Fig. 16 repeats the ensemble mean post- minus pre-1976 difference in the simulated precipitation for the GOGA runs but with boxes 1–4 added to indicate selected regions for a significance test. The histograms of area-averaged $\{\Delta P_k\}$ for the 4 boxes for the 48 members of the GOGA runs are shown in the lower panels in Fig. 16. All ensemble members simulated a positive ΔP_k for box 1 (Mexico and part of the southwest U. S.) and a negative ΔP_k for box 2 (northern South America), and all but one simulated a positive ΔP_k for box 3 (middle South America). Combining the ensemble mean, 0.24 mm/day, standard deviation, 0.086 mm/day, and the number of independent samples, $n=48$, for box 1, one can immediately infer by Student's t test (see e.g., the rule of thumb, Eq. 1, in Sardeshmukh et al. 2000) that the post- minus pre-1976 difference in precipitation for this box is greater than 0.2 mm/day at above 95% significance level. A similar test shows that the mean of ΔP_k is less than -0.52 mm/day for box 2 and greater than 0.23 mm/day for box 3, both at above 95% level. To provide a contrast, box 4 is chosen as a region with a small ensemble mean signal. Of the 48 members, 19 (29) simulated a negative (positive) ΔP_k . The ensemble mean, -0.004 mm/day, and standard deviation, 0.166 mm/day, indicate that the 48 samples are not enough to establish that the mean of ΔP_k is distinguishable from 0 at 95% level.

Appendix 3

Decomposing the interdecadal shift in a quadratic term

Defining the interdecadal shift in a single variable X across the 1976 transition as $\delta X \equiv [X]_{\text{POST}76} - [X]_{\text{PRE}76}$, we will derive an expression for the interdecadal shift in a quadratic quantity, XY . For clarity, a bracket, $[]$, is used in this appendix to indicate the mean of the post- or pre-1976 epoch. By definition (subscripts “POST” and “PRE” stand for post- and pre-1976),

$$\delta(XY) = [XY]_{\text{POST}} - [XY]_{\text{PRE}}. \quad (7)$$

For either the post- or pre-1976 period, the epoch mean of XY can be written as

$$[XY] = [X][Y] + [X^*Y^*], \quad (8)$$

where X^* is the year-to-year anomaly (departure from the epoch mean) of X due to interannual variability. Combining Eqs. 7 and 8, one obtains

$$\begin{aligned} \delta(XY) &= [X]_{\text{POST}}[Y]_{\text{POST}} + [X^*Y^*]_{\text{POST}} \\ &\quad - [X]_{\text{PRE}}[Y]_{\text{PRE}} - [X^*Y^*]_{\text{PRE}} \\ &= ([X]_{\text{PRE}} + \delta X)([Y]_{\text{PRE}} + \delta Y) \\ &\quad + [X^*Y^*]_{\text{POST}} - [X]_{\text{PRE}}[Y]_{\text{PRE}} \\ &\quad - [X^*Y^*]_{\text{PRE}} \\ &= (\delta Y)[X]_{\text{PRE}} + (\delta X)[Y]_{\text{PRE}} \\ &\quad + \delta X \delta Y + [X^*Y^*]_{\text{POST}} \\ &\quad - [X^*Y^*]_{\text{PRE}}. \end{aligned} \quad (9)$$

Reverting to the notation in Eq. 6, $[X]_{\text{PRE}}$ and $[Y]_{\text{PRE}}$ are X_C and Y_C . The last three terms in the r.h.s. of Eq. (9) are the “higher-order terms”. The $\delta X \delta Y$ term is smaller than the first two terms in the r.h.s. of Eq. (9) if $|X_C| \gg |\delta X|$, $|Y_C| \gg |\delta Y|$, which is generally true for horizontal velocity and specific humidity. The last two terms in Eq. 9 indicate that the difference between the interannual variability in the post- and pre-1976 periods could contribute to the difference in the epoch means (of a quadratic quantity) of the two periods. This contribution might not be negligible in the POGA-ML and GOGA runs and in observations, due to the presence of more strong El Niño events in the post-1976 era. By design, however, it is small for the SCYC runs considered in Sect. 4, since the “repeated seasonal cycle” experiments produce only weak and random interannual variability (see Fig. 11d). Thus, for the analyses in Sect. 4 for the SCYC runs, the last three terms in Eq. 9 are neglected as the higher-order terms. This is justified a posteriori as the sum of the four retained terms in Eq. 6 turns out to be very close to the total (compare Figs. 6e and 4c).

References

- Abarca del Rio R (1999) The influence of global warming in Earth rotation speed. *Ann Geophys* 17:806–811
- Alexander MA, Blade I, Newman M, Lanzante JR, Lau NC, Scott JD (2001) The atmospheric bridge: the influence of ENSO teleconnections on air-sea interaction over the global oceans. *J Climate* 15:2205–2231
- Allan RP, Slingo A, Ramaswamy V (2002) Analysis of moisture variability in the European Centre for Medium-Range Forecasts 15-year reanalysis over the tropical oceans. *J Geophys Res* 107:4230, 10.1029/2001JD001132
- Bates GT, Hoerling MP, Kumar A (2001) Central U.S. springtime precipitation extremes: teleconnections and relationship with sea surface temperature. *J Climate* 14:3751–3766
- Boer GJ, Yu B, Kim SJ, Flato GM (2004) Is there observational support for an El Niño-like pattern of future global warming? *Geophys Res Lett* 31: L06201, doi:10.1029/2003GL018722
- Cane MA, Clement AC, Kaplan A, Kushnir Y, Murtugude R, Pozdnyakov D, Seager R, Zebiak SE (1997) Twentieth century sea surface temperature trends. *Science* 275:957–960
- Cayan DR, Dettinger MD, Diaz HF, Graham NE (1998) Decadal variability of precipitation over western North America. *J Climate* 11:3148–3166

- Charney JG (1963) A note on large-scale motions in the tropics. *J Atmos Sci* 20:607–609
- Chiang JCH, Sobel AH (2002) Tropical tropospheric temperature variations caused by ENSO and their influence on the remote tropical climate. *J Climate* 15:2616–2631
- Chou C, Neelin JD (2004) Mechanisms of global warming impacts on regional tropical precipitation. *J Climate* 17:2688–2701
- Deser C, Phillips AS, Hurrell JW (2004) Pacific interdecadal climate variability: linkages between the Tropics and North Pacific during boreal winter since 1900. *J Climate* 17:3109–3124
- Fedorov AV, Philander SG (2001) A stability analysis of tropical ocean-atmosphere interaction: bridging measurements and theory for El Niño. *J Climate* 14:3086–3101
- Giannini A, Saravanan R, Chang P (2004) The preconditioning role of tropical Atlantic variability in the development of the ENSO teleconnection: implications for the prediction of Nordeste rainfall. *Clim Dyn* 22:839–855
- Gill AE (1980) Some simple solutions for the heat-induced tropical circulation. *Q J R Meteor Soc* 106:447–462
- Goddard L, Mason SJ, Zebiak SE, Ropelewski CF, Basher R, Cane MA (2001) Current approaches to seasonal-to-interannual climate predictions. *Int J Climatol* 21:1111–1152
- Gu DF, Philander SGH (1997) Interdecadal climate fluctuations that depend on exchanges between the tropics and extratropics. *Science* 275:805–807
- Hoerling MP, Kumar A (2003) The perfect ocean for drought. *Science* 299:691–694
- Hoerling MP, Hurrell JW, Xu T (2001) Tropical origins for recent North Atlantic climate change. *Science* 292:90–92
- Hsu HH, Lin SH (1992) Global teleconnections in the 250-mb streamfunction field during the Northern Hemisphere winter. *Mon Weather Rev* 120:1169–1192
- Huang HP, Weickmann KM, Hsu CJ (2001) Trend in atmospheric angular momentum in a transient climate change simulation with greenhouse gas and aerosol forcing. *J Climate* 14:1525–1534
- Huang HP, Weickmann KM, Rosen RD (2003) Unusual behavior in atmospheric angular momentum during the 1965 and 1972 El Niño. *J Climate* 16:2526–2539
- Kaplan A, Cane M, Kushnir Y, Clement A, Blumenthal M, Rajagopalan B (1998) Analyses of global sea surface temperature 1856–1991. *J Geophys Res* 103:18567–18589
- Karspeck AR, Seager R, Cane MA (2004) Predictability of tropical Pacific decadal variability in an intermediate model. *J Climate* 17:2842–2850
- Kinter III JL, Fennessy MJ, Krishnamurthy V, Marx L (2004) An evaluation of the apparent interdecadal shift in the tropical divergent circulation in the NCEP-NCAR reanalysis. *J Climate* 17:349–361
- Knutson TR, Manabe S (1995) Time-mean response over the tropical Pacific to increased CO₂ in a coupled ocean-atmosphere model. *J Climate* 8:2181–2199
- Kumar A, Yang F, Goddard L, Schubert S (2004) Differing trends in the tropical surface temperatures and precipitation over land and oceans. *J Climate* 17:653–664
- Lau NC, Leetmaa A, Nath MJ, Wang HL (2005) Influences of ENSO-induced Indo-Western Pacific SST anomalies on extratropical atmospheric variability during the boreal summer. *J Climate* (in press)
- Levitus SE, Boyer T (1994) World ocean atlas 1994, vol 4: temperature, NOAA Atlas NESDIS 4, U. S. Department of Commerce, Washington
- McPhaden MJ, Zhang D (2002) Slowdown of the meridional overturning circulation in the upper Pacific Ocean. *Nature* 415:603–608
- Nakamura H (1993) Horizontal divergence associated with zonally isolated jet streams. *J Atmos Sci* 50:2310–2313
- Neelin JD, Chou C, Su H (2003) Tropical drought regions in global warming and El Niño teleconnections. *Geophys Res Lett* 30:doi:10.1029/2003GL018625
- Peixoto JP, Oort AH (1992) Physics of climate. American Institute of Physics, New York, p 520
- Qin J, Robinson WA (1993) On the Rossby wave source and the steady linear response to tropical forcing. *J Atmos Sci* 50:1819–1823
- Rayner NA, Parker DE, Horton EB, Folland CK, Alexander LV, Rowell DP, Kent EC, Kaplan A (2003) Global analyses of sea surface temperature, sea ice, and night marine air temperature since the late nineteenth century. *J Geophys Res* 108:Art. No. 4407
- Robinson WA (1994) Comments on “Horizontal divergence associated with zonally isolated jet streams”. *J Atmos Sci* 51:1760–1761
- Robinson WA (2002) On the midlatitude thermal response to tropical warmth. *Geophys Res Lett* 29:doi:10.1029/2001GL014158
- Ropelewski CF, Halpert MS (1987) Global and regional scale precipitation patterns associated with the Southern Oscillation. *Mon Weather Rev* 115:1606–1626
- Russell GL, Miller JR, Tsang LC (1985) Seasonal oceanic heat transports computed from an atmospheric model. *Dyn Atmos Oceans* 9:253–271
- Sardeshmukh PD, Hoskins BJ (1988) The generation of global rotational flow by steady idealized tropical divergence. *J Atmos Sci* 45:1228–1251
- Sardeshmukh PD, Compo GP, Penland C (2000) Changes of probability associated with El Niño. *J Climate* 13:4268–4286
- Schneider EK (1987) A simplified model of the modified Hadley circulation. *J Atmos Sci* 44:3311–3328
- Schneider EK, Bengtsson L, Hu ZZ (2003) Forcing of Northern Hemisphere climate trends. *J Atmos Sci* 60:1504–1521
- Schubert SD, Suarez MJ, Pegion PJ, Koster RD, Bacmeister JT (2004) Causes of long-term drought in the United States Great Plains. *J Climate* 17:485–503
- Seager R, Harnik N, Kushnir Y, Robinson W, Miller J (2003) Mechanisms of hemispherically symmetric climate variability. *J Climate* 16:2960–2978
- Seager R, Karspeck A, Cane M, Kushnir Y, Giannini A, Kaplan A, Kerman B, Miller J (2004) Predicting Pacific decadal variability. In: Wang C, Xie S-P, Carton J (eds) *Earth Climate: The Ocean-Atmosphere Interaction*. American Geophysical Union, Washington, pp 105–120
- Seager R, Harnik N, Robinson WA, Kushnir Y, Ting M, Huang HP, Velez J (2005) Mechanisms of ENSO-forcing of hemispherically symmetric precipitation variability. *Q J R Meteorol Soc* (in press)
- Smith TM, Reynolds RW, Livezey RE, Stokes DC (1996) Reconstruction of historical sea surface temperatures using empirical orthogonal functions. *J Climate* 9:1403–1420
- Thompson DWJ, Wallace JM, Hegerl GC (2000) Annular modes in the Extratropical circulation, part II: trends. *J Climate* 13:1018–1036
- Trenberth KE (1990) Recent observed interdecadal climate changes in the Northern Hemisphere. *Bull Amer Meteor Soc* 71:988–993
- Trenberth KE, Branstator GW, Karoly D, Kumar A, Lau NC, Ropelewski C (1998) Progress during TOGA in understanding and modeling global teleconnections associated with tropical sea surface temperature. *J Geophys Res* 103:14291–14324
- Trenberth KE, Stepaniak DP, Hurrell JW, Fiorino M (2001) Quality of reanalysis in the tropics. *J Climate* 14:1499–1510
- Webster PJ, Holton JR (1982) Cross equatorial response to middle-latitude forcing in a zonally varying basic state. *J Atmos Sci* 39:722–733
- Yulaeva E, Wallace JM (1994) The signature of ENSO in global temperature and precipitation fields derived from the microwave sounding unit. *J Climate* 7:1719–1736